Modeling Solar Generation during Hurricanes[†]

Luis Ceferino,[*,‡,¶] Ning Lin,[‡,¶] and Dazhi Xi[¶]

‡*The Andlinger Center for Energy and the Environment, Princeton University*

¶*Department of Civil and Environmental Engineering, Princeton University*

E-mail: *lceferinor@gmail.com

Abstract

Because solar generation adoption shows unprecedented growth, our power systems may extensively rely on solar generation infrastructure as the primary source of modern and clean energy in just a few decades. Despite this growth, very few studies have captured solar generation infrastructure's behavior during natural disasters to understand their real benefit for resilience. Here, we present an integrative methodology to quantify solar generation during hurricanes. The methodology combines a hurricane hazard model, solar irradiance quantification, solar panel vulnerability, and a model for irradiance decay during hurricane conditions. We develop the irradiance decay model through a mixed-effect regression on a dataset that merges historical Global Horizontal Irradiance and the revised data of Atlantic hurricane activity. The methodology is applied to 21 states in the Eastern U.S. for different extreme events. Our results show that for events with return periods of up to 33 years, the loss in generation stems from cloud conditions during hurricanes. However, less frequent events can cause solar panel failure, especially in southern regions of the U.S., triggering complete loss of solar generation. Given that solar generation is expected to grow significantly, these results advocate for higher standards in the structural design of solar panels.

[†]Preprint submitted to Journal of Environmental Science and Technology

Synopsis: New methodology to model solar generation during hurricanes shows substantial regional variability in the resilience of modern power systems in the U.S..

Keywords: Disaster resilience; solar panels; distributed energy resources; hurricanes; climate change.

Introduction

Solar generation is becoming a pillar in modern power systems. Solar energy accounted for nearly 40% of all the new electric generating capacity installed on the U.S. grid in 2019, the highest share in its history.[1] The rapid adoption of panels to harvest solar energy is transforming the power system economics, environmental contributions to global warming, and resilience.[2] Research has already highlighted and projected solar energy's long-term environmental[3,4] and economic[5,6] benefits. However, there is significantly less understanding of solar infrastructure's disaster vulnerability and its actual impact on the power system's resilience, which often reveals its extensive vulnerabilities through massive outages during natural disasters. For example, Hurricane Maria in 2017 left millions of people without power in Puerto Rico,[7] and so did the recent 2019-2020 wildfires in California.[8,9]

Current research has mainly focused on quantifying the resilience of traditional power systems to natural disasters.[10–14] These investigations have not accounted for the vulnerability of solar energy infrastructure or generation decentralization, a fundamental paradigm switch where users can generate energy locally, e.g., rooftop solar panels. Only a recent investigation has proposed a framework to quantify the resilience of modern power systems with rooftop solar panels,[15,16] but exclusively for earthquake hazards. As hurricanes pose an enormous threat to urban centers worldwide, this paper investigates modern power systems' resilience with solar infrastructure during hurricanes.

Unlike earthquakes, hurricanes cause wind damage to solar infrastructure and only occur in seasons when solar irradiance and generation are high. Additionally, hurricanes bring environmental conditions that may drastically reduce solar irradiance, which has not been

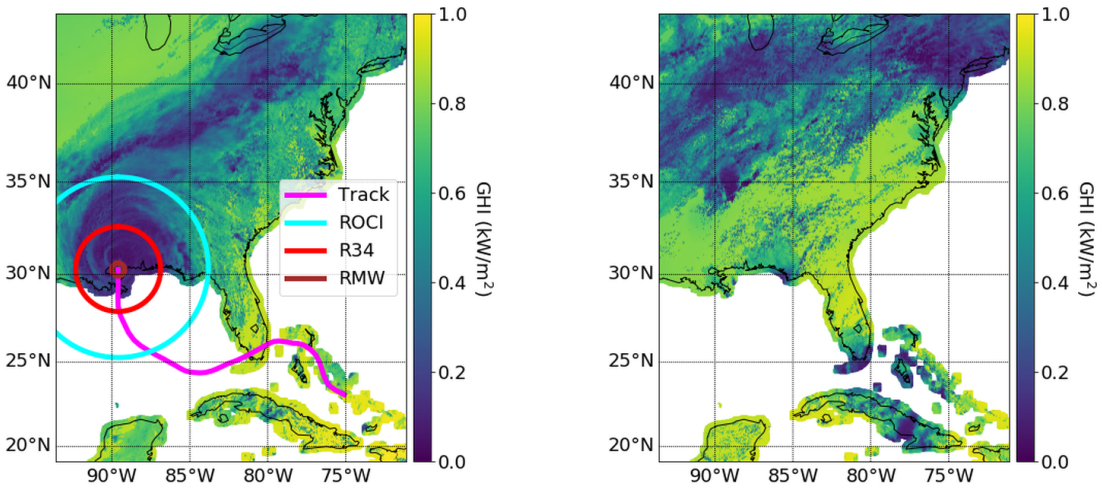

(a) 2005 (during hurricane Katrina)

(b) 2006 (one year after hurricane Katrina)

Figure 1: Global horizontal irradiance decay during hurricanes with two snapshots at the same time but in different years. Both plots show the spatial distribution of GHI on August 29th, at 3 pm UTC (or 10 am local time in Lousiana). (a) The plot shows GHI in 2005 during Hurricane Katrina, indicating the hurricane's track, radius of maximum wind, radius at a wind speed of 34 knots, and radius of the outermost closed isobar. (b) The plot shows GHI in 2006 in the same region at the same time. Data retrieved from NREL.[17]

addressed by the existing literature. Figure 1 exemplifies the effect of hurricanes on the spatial distribution of solar irradiance by showing Global Horizontal Irradiance (GHI) at 3pm UCT (9 am local time) when Hurricane Katrina made landfall in Louisiana as a category 3 event in 2005 compared to the GHI distribution the year after. The comparison shows that the hurricane reduced GHI even for sites that were hundreds of kilometers away from the hurricane center.

To fill this research gap, we conduct an extensive data analysis on historical GHI during the hurricane seasons from 2001 to 2017 by combining the hurricane Best Track Database[18] with a GHI database from the National Renewable Energy Laboratory (NREL).[17] The analysis identifies hurricane features that best predict the intensity and extent of GHI decay. We fit different functional forms for GHI decay during hurricane conditions and highlight the best predictive model.

Next, the paper proposes an integrative framework to quantify solar generation during

hurricanes. We use synthetic storm data generated with statistical and physics-based tropical cyclone simulations for current atmospheric and oceanic environments.[19,20] We utilize a physics-based model to estimate the storms' wind fields[21] and couple the fields with recently developed wind-based fragility functions for solar panels[22,23] to estimate wind damage to panels. Then, the integrative framework uses probabilistic models to transform estimates of GHI during normal conditions[17] to hurricane conditions. The transformation uses our proposed model for GHI decay during hurricanes in multiple regions of the U.S. at different times of the day and throughout the entire hurricane season. The integrative framework uses an algorithm based on Monte Carlo simulation to quantify the time-series of solar generation.

Finally, we apply the framework to quantify power generation from solar panels in the Eastern U.S.. We discuss the results as well as regional variations of the contributions of solar panels to power generation resilience through different counties. With these novel models and geographically-extensive case study, this paper lays the groundwork to quantify the resilience of power systems with solar infrastructure to hurricanes.

Material and Methods

Collecting data for GHI during previous hurricanes

Hurricane conditions reduce solar irradiance intensity at the ground level over large geographical extents, limiting the ability of PV panels to harvest energy in communities. Figure 1 shows intense GHI decays during Hurricane Katrina in most regions within the radius (R34) at a wind speed of 17 ms^{-1} (34 knots), which reached 262 km. In some regions, intense decays extended to distances similar to the radii of the outermost closed isobar (ROCI), which reached 556 km. While Figure 1 shows only a snapshot for one hurricane demonstrating irradiance decays, we consistently observe the same trend in other hurricanes. In contrast to cloudless conditions of clear skies, which are associated with maximum solar generation, hurricanes cover extensive regions with different cloud structures from the eyewall to the

rainbands.[24] These clouds absorb and scatter light, reducing direct incident radiation and generally leading to lower GHI and reduced solar panel generation.[25,26] Clouds that have high moisture density and vertical depth, i.e. optically thick clouds, can drastically reduce direct incident radiation.[27] Accordingly, hurricanes can significantly and rapidly lessen generation through optically thick cloud structures such as large cumulonimbus. However, hurricanes can also reduce generation significantly even with less optically thick cloud structures like stratiform clouds because they can cover large geographical extents.

To systematically investigate the effect of hurricanes on irradiance, we coupled a large dataset of GHI with historical hurricane data. We used the Physical Solar Model (PSM) version 3 from the National Solar Radiation Database (NSRDB) published by the National Renewable Energy Laboratory (NREL) to extract GHI with high spatial and temporal resolution.[17] The PSM combines satellite-derived atmospheric and land surface properties with radiative transfer models to solve solar radiation through the Earth's atmosphere. The PSM provides solar irradiance at a 4-km horizontal resolution for 30-minute intervals from 1998 to 2017. The PSM enable us to observe the GHI behavior at different timesnaps for different hurricanes since 1998 for multiple sites and under various hurricane conditions.

Hurricane dataset

We compiled hurricane data from the revised Atlantic hurricane database (HURDAT2).[18] The data contain multiple hurricane features and span several decades; however, key spatial information including hurricanes' radii is only available since 1998. The hurricane data include ROCI, the radius of maximum wind (RMW), radius at wind speeds of 17 ms^{-1} (R34, 34 knots) and 33 ms^{-1} (R64, 64 knots), hurricane category, and maximum wind speeds. The hurricane data have a 3-hour temporal resolution, which is coarser than the PSM temporal resolution; thus, we reduced the granularity of the GHI dataset from 30 minutes to 3 hours and matched the hurricane recording times. After performing a preliminary assessment to estimate the geographical extent impacted by the hurricane, we collected GHI records from

the 4×4-km spatial grid within two times ROCI from the hurricane center, which reached several hundreds of kilometers for massive storms.

We analyzed 22 landfalling hurricanes whose geneses were in the North American basin and whose lifetime maximum intensity reached a category of at least 3 to filter out the disproportionately large number of storms that do not reach high intensities. The 22 hurricanes cover an extensive geographical region of our assessment (Figure S1). These hurricanes have a wide variety of conditions, with maximum wind speeds up to 80 ms^{-1} (category 5), ROCI from 200 km to above 800 km, RMW up to 250 km, and radii at circulating wind speeds of 0 (R0) from 200 km to above 2000 km (Figure S2). HURDAT2 omitted R0, the shortest distance where hurricane circulating wind effects dissipate entirely. [1] Thus, we estimated R0 with a wind profile model that captures the radial structure of tropical cyclones.[21]

Key features for predicting GHI during hurricanes

To characterize GHI decay under different hurricane conditions, we define I^h as GHI during a hurricane. Previous research shows that GHI has strong temporal and spatial variability during normal conditions, i.e., no hurricane.[15,28] We account for such variability and characterize GHI deviations from normal conditions in the logarithm space as

$$\delta^h = ln\left(\frac{I^h}{\bar{I}}\right) \tag{1}$$

where $\bar{I}$ represents the median of the GHI under normal conditions at the same location and at the same time of the year as I^h. We used 20 years of GHI data to estimate $\bar{I}$ for all the geographical extent covered by the hurricanes using a 3-hour temporal resolution. We assume that at each time of the day, GHI has approximately the same distribution for a given month. As a result, we used approximately 600 instead of 20 data points to estimate the GHI medians. For example, to estimate GHI at 10 a.m. in June, we lumped the data of

[1] Notice that there is environmental wind at R0.

its days from 1998 to 2017. We observe that for sites farther from the center of the hurricane, the median of δ^h approaches zero, implying that the site is outside the area where hurricanes reduce GHI, i.e., $\bar{I} = \overline{I^h}$.

We analyzed GHI during the 22 hurricanes to estimate the samples $\widehat{\delta^h}$ and understand GHI behavior during different hurricane conditions. Because our focus was only on times of the day when communities can generate energy, we only included in our analysis daytime data where and when $\bar{I} > 10$ W-h/m^2, which finally resulted in ∼28M data points. Figure 2 shows $\widehat{\delta^h}$ as a function of distance from the site to the hurricane's center and category.

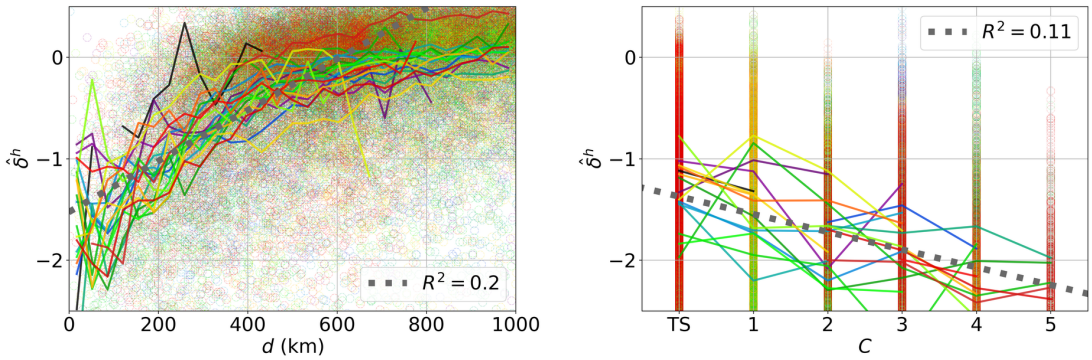

(a) Distance to the center

(b) Category (TS: Tropical storm)

Figure 2: Scatter plots showing relationship between GHI decay and key hurricane features. $\widehat{\delta^h}$ during different hurricanes have different color. For each hurricane, the plots show a running mean for $\widehat{\delta^h}$ using solid lines. The plots also show linear regressions in dotted lines and their corresponding R^2 values when the multi-hurricane data is lumped together. For visual clarity, there are only 50k randomly sampled data points in each plot.

Figure 2a shows the relationship between distances to the hurricane center d and $\widehat{\delta^h}$. On average, $\widehat{\delta^h}$ has reduced values for small d and grows steadily up to a plateau close to 0 for d values larger than 600 km. We fitted a line with d below 600 km to account mainly for the sites with significant irradiance decays and found an R^2 of 0.2 (correlation $\rho = 0.45$). We observe that the fitted line is not able to represent the transition between small distances

to the plateau for large d where hurricanes have little effect. The observed transition is consistent with the spatial distribution of cloud optical thicknesses in hurricanes. Hurricane eyewalls, which surround the hurricane eye typically at 10-50 km from the center,[29] are composed of optically thick clouds as a result of high moisture densities and large vertical depths,[30,31] thus significantly reducing direct incident radiation through high absorption and reflection. Outside the eyewall, clouds' optical thicknesses are high only in rainbands and significantly lower in between them. Outside the regions with rainbands, a regular combination of clear-sky and partially cloudy conditions arise, bringing GHI back to normal levels.[30–32] Figure 2a shows that this occurs beyond 600 km from the hurricane center.

Additionally, we find that high hurricane intensity exacerbates GHI decay. To focus on sites with the largest hurricane decay and cover areas within hurricane eyewalls, we analyzed sites located at 100km or less from the hurricane center. Figure 2b shows a decaying trend between hurricane category C and averaged $\widehat{\delta^h}$ values, indicating that more intense hurricanes induce larger reductions in solar irradiance. A similar trend is observed between $\widehat{\delta^h}$ and maximum winds V (Figure S3a) because V has high colinearity with C as the latter variable is an increasing step function of V. Thus, we see that the linear fit performs very similarly with R^2 of nearly 0.11 (ρ = -0.34) in both cases. Lower irradiance levels for higher hurricane categories are also consistent with recent evidence on satellite-derived cloud microphysical features during hurricanes.[31] There are larger regions with higher cloud optical thicknesses associated with large and thick cloud structures such as cumulonimbus during hurricane maturity and intensification rather than during hurricane development or dissipation.

To capture hurricane size effect, we evaluated the relationship between different relevant hurricane radii and both the intensity and geographical extent of GHI decay. To study whether GHI decays are larger for bigger hurricanes, we analyzed the relationship between $\widehat{\delta^h}$ and ROCI, RMW, and R0, respectively. We observe that hurricane size does not intensify GHI decay as linear fits have low R^2 values of 0, 0.05, and 0.02, respectively (Figure S3).

To study how hurricane size correlates with the geographical extent of GHI decay, we

analyzed the relationship between GHI and distance to the storm's center normalized by the hurricane size. We normalized d by four hurricane size metrics, ROCI, RMW, R0, and R34, where R34 is the radius at which the maximum wind speed is 34 knots, the minimum speed for the event to be categorized as a tropical storm. We split the data by hurricane category because C showed predictive power for hurricane decay intensification (Figure 2).

When the distance is normalized by ROCI and R34, we generally observe better fitting performance than for the absolute distance, with improved performance for higher hurricane categories (Figure S4 and S7). We estimated that a linear fit between $R = d/\text{ROCI}$ and $\widehat{\delta}^h$ has an R^2 of 0.38 for category 5, almost twice the value found for absolute distance (Figure 2a). For $R = d/\text{R34}$, R^2 values show comparably good fitting performance to using ROCI as normalizing distance (Table S1). The slopes of linear fits are steeper for higher categories, further demonstrating that the intensity of the hurricane intensifies GHI decay (Figure S4 and S7). As discussed earlier, this feature of GHI decay is driven by optically thicker cloud structures occurring during hurricane maturity and intensification. Distances normalized by RMW and R0 give lower performance, which, however, still illustrate how the effect of the hurricane on irradiance dissipates for large enough values of d (Figure S5 and S6).

The analysis also shows that the regions with GHI decay easily extend beyond RMW and R34 as they only define hurricanes' inner-core circulation (Table S1). In contrast, it also shows that the regions with significant GHI decay do not reach R0 but are close to being bounded by ROCI. Thus, these observation suggests that the outer structure and radial extent of circulation bounded by ROCI is coupled with the cloud structures absorbing and reflecting light during hurricanes.

Probabilistic model for GHI during hurricanes

To leverage well-established mixed-effects regression models,[33] we assume that $ln(I^h)$ is Gaussian, i.e., I^h is lognormaly distributed, during daytime, when generation is not negligible, i.e., $I^h > 0$. Thus

$$ln(I^h) = ln\big(\overline{I^h}\big) + \epsilon^h \tag{2}$$

where $\overline{I^h}$ is the GHI median, and ϵ^h is a Gaussian random variable with zero mean that accounts for the variability of GHI during hurricanes in the logarithmic space. We also assume that hurricanes reduce median GHI from normal conditions to $\overline{I^h}$ such that in the logarithmic space

$$ln(I^h) = ln(\bar{I}) + f(R, C) + \epsilon^h \tag{3}$$

where $\bar{I}$ is the median GHI during normal conditions, and $f(R, C)$ is a reduction factor that is function of the normalized distance to the hurricane's center R and the hurricane category C. f uses both R and C because they demonstrated to have good predictive power for GHI decay in the previous section. Using the expression in Equation 1, then

$$\delta^h = f(R, C) + \epsilon^h \tag{4}$$

Using Equation 4 and the samples of δ^h from our dataset, we conducted a mixed-effect regression analysis to test multiple functional forms $f(R, C)$ and formulate a predictive model for irradiance decay during hurricanes.

Functional Forms for f: We tested four different functional forms for $f(R, C)$. These functional forms are shown in Equation 5. All of them include a logarithmic growth as a function of R followed by a plateau when $f(R, C)$ reaches 0. The functional forms include a short-distance correction factor b and a scale factor c that further calibrate the influence of R on the irradiance decay. The short-distance correction factor is added to the value of R so that the logarithmic function approaches the observed values rather than $-\infty$ when the site is close to the center of the hurricane, i.e., $R \to 0$. The scale factor further normalizes R to define where the plateau is reached.

While all of the functional forms include a slope that varies with the hurricane category

$(a_1C + a_2)$, they vary in their complexity, differing in the representation of the short-distance correction factor b and the scale factor c. In the functional form f_1 in Equation 5a, b and c remain constant for all hurricane categories. In the functional form f_2 in Equation 5b, b varies with category but c remains constant, and in the functional form f_3 in Equation 5c, b is constant and c varies with hurricane category. In the functional form f_4 in Equation 5d, both b and c vary with hurricane category.

$$f_1(R,C) = \begin{cases} (a_2C + a_1) \times ln\left(\frac{R+b}{c}\right) & \text{if } R + b < c \\ 0 & \text{if } R + b \geq c \end{cases} \tag{5a}$$

$$f_2(R,C) = \begin{cases} (a_2C + a_1) \times ln\left(\frac{R+(b_2C+b_1)}{c}\right) & \text{if } R + (b_2C + b_1) < c \\ 0 & \text{if } R + (b_2C + b_1) \geq c \end{cases} \tag{5b}$$

$$f_3(R,C) = \begin{cases} (a_2C + a_1) \times ln\left(\frac{R+b}{c_2C+c_1}\right) & \text{if } R + b < c_2C + c_1 \\ 0 & \text{if } R + b \geq c_2C + c_1 \end{cases} \tag{5c}$$

$$f_4(R,C) = \begin{cases} (a_2C + a_1) \times ln\left(\frac{R+(b_2C+b_1)}{c_2C+c_1}\right) & \text{if } R + (b_2C + b_1) < c_2C + c_1 \\ 0 & \text{if } R + (b_2C + b_1) \geq c_2C + c_1 \end{cases} \tag{5d}$$

Mixed-Effects Regression for GHI decay: We used a mixed-effects regression to capture the main observed features of irradiance decay during hurricanes. Unlike other methods like fixed-effects regression, this regression allows us to explicitly decompose the random variable ϵ^h in Equation 4 into two independent factors,[33] one factor accounting for the variability between different time steps represented by the random variable η^h and another accounting for the spatial variability at a fixed time represented by the random variable ε^h.

$$\delta^h = f(R,C) + \eta^h + \varepsilon^h \tag{6}$$

Through this explicit decomposition, we properly represent the high GHI temporal and

temporal variability structrure as extensively discussed in previous research.[15,28] The mixed-effects regression has both fixed and random components.[33] With the fixed effect component, we capture how hurricanes decrease (the logarithm of) median GHI with the factor $f(R, C)$ (Equation 5). With the random component of the regression, we capture spatial uncertainty at a time step with a within-time random effect ε^h and uncertainty across time steps with a between-time step random effect η^h. The regression assumes that η^h and ε^h are independent. Similar techniques and independence assumptions have been used to model natural disaster intensities with radiating decay. For example, random effect regressions and similar independence assumptions are extensively used to assess ground shaking that propagates from an earthquake epicenter to a large geographical extent.[34,35]

We lumped all hurricane data to fit the parameters of $f(R, C)$. Notice that for a fixed time t, an observation of δ^h at site j ($\delta^h_{t,j}$) is the sum of a realization of η^h and $\varepsilon^h_{t,j}$. As η^h_t only captures temporal uncertainty, at a fixed time t, it takes the same value for all sites. $\varepsilon^h_{t,j}$ captures spatial uncertainty, thus at fixed time t, it varies for each specific site j. Similarly, while C varies at each time step t, R also varies for each site j. Thus, for each observation

$$\delta^h_{t,j} = f(R_{t,j}, C_t) + \eta^h_t + \varepsilon^h_{t,j} \tag{7}$$

As described previously, we estimated $\delta^h_{t,j}$ for around $\sim$28 M observations corresponding to multiple time steps and sites of GHI recordings during the 22 hurricanes in the NREL dataset. We preprocessed the data by removing sites at long distances from the hurricane center, where hurricanes did not have significant effect on GHI. We then balanced the observations across the hurricane categories and distances from the center to the sites (see Supporting Information). Following these constraints, we used ~ 0.75 M data points for the analysis.

We estimated the model parameters using maximum likelihood estimation (MLE) for the non-linear mixed-effects regression with a Matlab package. The package uses an expectation-maximization algorithm to solve for the parameters of the fixed component in Equation 5

while accounting for the unobserved component of the regression in Equation 4.[36] We fitted the parameters for the four models considering the four previously analyzed normalization radii, ROCI, RMW, R0, R34.

Modeling solar generation during hurricanes

We propose an integrative algorithm that couples our proposed GHI decay model with synthetic hurricane simulations and a fragility function for rooftop solar panels. We used a synthetic dataset wtih 5018 physically possible landfalling storms in the U.S. generated from a statistical-deterministic tropical cyclone (TC) model.[19] The model accounts for current climate conditions according to the National Centers for Environmental Prediction (NCEP) reanalysis. As a result, the 5018 synthetic storms roughly correspond to 1485 years of simulation. The model consists of three parts: a random seeding genesis model, a beta-advection TC motion model, and a dynamical TC model that captures how environmental factors influence the intensity axisymmetric TCs. The model outputs TC locations, maximum sustained winds and radii of maximum winds in 2-hour intervals.

Additionally, at each time step, we estimate R0 based on both the radius of maximum wind and maximum wind using a TC wind field profile model that connects the inner storm structure to the outer structure.[21] We estimate ROCI using the expression ROCI $= 0.18 \times$ R0 $+ 226$ (km), which was obtained conducting a regression on the historic hurricane data. Wind fields are estimated by combining axisymmetric winds circulating counterclockwise from the TC wind profile model[21] and the background wind field.[37] Previously, this synthetic storm model has been extended to quantify TC surge[20] and TC rainfall,[38] demonstrating its versatility for multiple hurricane hazard assessments. Here, we extend the applicability of the TC model to quantify solar generation during hurricanes.

Fragility function of solar panels

We used a fragility function developed according to current structural design standards for solar panels.[22] The wind measure in the fragility function was transformed from 3-second gust to 1-minute sustained wind speeds to make it compatible with the synthetic hurricane data using an empirical formula.[39] Hurricanes of category 3, starting at maximum wind speeds of 50 ms^{-1} (3-second gusts of 60 ms^{-1}), can induce failure with a likelihood higher than 50% (Figure S10).

Algorithm to estimate cumulative solar generation during hurricanes

We based our assessment on Monte Carlo simulation. The algorithm analyzes H realizations of hurricanes and estimates solar generation for each site j (out of N sites of interest) during multiple time steps t. First, the panel damage state s is represented by a Bernoulli distribution. s takes the value of 1 if the hurricane causes solar panel failure due to extreme wind conditions or 0 otherwise. Thus

$$s \sim \text{Bernoulli}(p) \tag{8a}$$

$$p = \Phi\left(\frac{\ln(\max_t(w_{t,j})) - \ln(\bar{w})}{\beta}\right) \tag{8b}$$

where $\Phi(.)$ is the standard normal cumulative distribution function, $\max_t(w_{t,j})$ is the maximum wind that the solar panel at site j experiences during the hurricane, and $\bar{w}$ and β equal 58 ms^{-1} (3-second maximum wind) and 0.3, respectively (Figure S8). Then, for a site j, a realization $\tilde{s_j}$ is sampled from Equation 9. Next, we explicitly model the panel failure time because this key variable will account for the energy that the panel will be able to generate before becoming nonfunctional. If there is panel failure, i.e., $\tilde{s_j} = 1$, we

model failure time τ with the probability density function $g_\tau(t)$. To account for higher likelihoods of failure when winds are more intense, we consider that $g_\tau(t)$ is proportional to the time-varying failure likelihood due to different wind conditions at the site throughout the hurricane. Thus, $g_\tau(t) \propto p_{t,j}$, where $p_{t,j}$ can be estimated from Equation 8b. Accordingly, at site j, a realization $\tilde{\tau}_j$ is sampled from $g_\tau(t)$ if $\tilde{s_j} = 1$, or it is assigned ∞ if $\tilde{s_j} = 0$, i.e., when the hurricane does not cause panel failure. At each time step t, the panel's time-varying functionality status $\tilde{x}_{t,j}$ is estimated as

$$\tilde{x}_{t,j} = \begin{cases} 0 & \text{if } t > \tilde{\tau}_j \\ 1 & \text{if } t \leq \tilde{\tau}_j \end{cases} \tag{9}$$

After assessing solar panel functionality, the algorithm samples GHI realizations. Following Equations 3 and 6,

$$I^h = \bar{I} \times e^{f(R,C)+\epsilon^h} \tag{10}$$

In the logarithmic space, ϵ^h accounts for spatiotemporal variability in GHI during hurricanes. Under our initial assumption that hurricanes only modify the GHI logarithmic mean, ϵ^h remains the same as normal-conditions ϵ. Thus

$$I^h = \bar{I} \times e^{f(R,C)+\epsilon} \tag{11}$$

Following the lognormality assumption for GHI under normal conditions, I^h can be estimated by transforming GHI during normal conditions to GHI during hurricane conditions

$$I^h = I \times e^{f(R,C)} \tag{12}$$

Based on the assumption that hurricanes only modify the GHI logarithm mean, Equation 12 enables us to leverage well-defined GHI normal condition statistics throughout the entire U.S.[17] with a clean and simple formula to find decayed GHI during hurricanes. For each site

j and time t, a realization of GHI during normal conditions ($\tilde{I}_{t,j}$) is sampled and adjusted to hurricane conditions using $f(R_{t,j}, C_t)$ as

$$\tilde{I}^h_{t,j} = \tilde{I}_{t,j} \times e^{f(R_{t,j}, C_t)} \tag{13}$$

Next, the power $\tilde{q}_{t,j}$ generated at time t and site j is estimated per area of installed solar panel A with efficiency E, the ratio between the amount of electricity the panel produces and the amount of solar energy it absorbs from the sun. Thus

$$\tilde{q}_{t,j} = \tilde{I}^h_{t,j} \times \tilde{x}_{t,j} \times A \times E \tag{14}$$

Finally, the cumulative energy $\tilde{Q}_{t,j}$ generated is updated by adding the product between $\tilde{q}_{t,j}$ and dt, the interval between time steps.

$$\tilde{Q}_{t,j} = \tilde{Q}_{t-1,j} + \tilde{q}_{t,j} \times dt \tag{15}$$

Results

Best-Fitted functions for GHI decay

We conducted mixed-effect regressions for all 16 combinations of functional forms and normalizing radii. We report all fitted parameters in the Supplementary Information. Additionally, we estimated the Akaike information criterion (AIC)[40] to evaluate the regressions' relative statistical performance. The model with f_4 and $R = d/\text{ROCI}$ exhibits the best performance. We find that the selection of the functional form f did not modify the regression statistical performance to the degree of the selection of the normalizing radius. The performance of ROCI is followed by R34, and ROCI and R34 performed significantly better than RMW and R0 (see Supplementary Information).

Figure 3 shows the best fit, that is, f_4 and $R = d/\text{ROCI}$, for different categories. The

plot shows how GHI decays during hurricanes, with stronger effects closer to the hurricane center and for higher hurricane categories. These observations are consistent with the presence of optically thick cloud structures close to the hurricane center and during hurricane maturity and intensification as noted previously. The regression also shows that the decay consistently extends up to sites that are ∼1.3 times ROCI from the hurricane center, confirming the observation that the cloud structures and radial extent of hurricane circulation defined by ROCI are strongly coupled with the hurricane mechanism for high light absorption and reflection. Because this threshold (~ 1.3) does not change significantly for different categories, hurricanes with low categories can cover more extensive regions with clouds that reduce GHI than hurricanes with high categories as long as they have larger ROCI. However, the level of the decay will be smaller for lower categories.

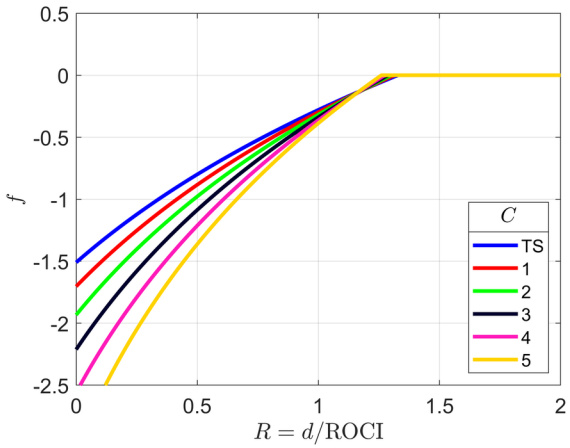

Figure 3: Fitted f_4 as function of $R = d/\text{ROCI}$ that tracks GHI decay during hurricanes. This fit has the best AIC performance out of the 16 combinations of normalizing radii and functional forms tested.

Solar generation in the East Coast of the U.S. during hurricanes

We use our integrative framework to estimate the distribution of cumulative solar generation during hurricanes in 1217 counties of 21 states with high hurricane risk in the East Coast of the U.S.. The 5018 synthetic hurricanes described previously were included in the assessment ($H = 5018$). We used the counties' centroids as sites of interest ($N = 1217$) and conducted

the analysis for unitary area of installed solar panel ($A = 1$) and for an efficiency of 19% ($E = 0.19$), representative of the efficiency of commercial rooftop systems such as LG solar panels.

We assessed cumulative solar energy generation for four days during a hurricane emergency using time steps of 2 hours. In Figure 4, we show a subset of cumulative generations $\hat{Q}_{t,j}$ for four coastal counties exposed to high hurricane hazard, Galveston (TX), Miami (FL), New Hanover (NC), and New York (NY). Each curve depicts how much energy a stakeholder will harvest since a hurricane hits land. Thus, for $t = 0$ at landfall, we set $\tilde{Q}_{0,j}$ to 0 for all sites j. The gray curves show the simulations of cumulative electricity generation per square meter of installed solar panel due to different GHI levels during the hurricane season, GHI decay as a result of hurricane cloud conditions, and the potential failure of solar panels due to wind damage. For reference, the plots include in dashed and dotted lines cumulative solar generation from median GHI conditions during normal summer and winter seasons, respectively. The curves are wavy as GHI varies at different times of the day, i.e., the curves are flat at nights. Additionally, we evaluated the extreme hurricane conditions that led to low electricity generation in these counties and characterized them through return periods. While return periods are commonly estimated as a function of hurricane intensity,[41] in this application, we estimate return periods as function of cumulative solar generation, our metric for resilience. For a certain generation level, we estimated its return period as the division between the number of equivalent years of hurricane simulation (1485) and simulated events with same or worse generations. These estimated return periods represent the average time between storms under which cumulative solar generation is below specific values. Storms that cause lower generation will have longer return periods.

Counties are more frequently affected by storms whose induced GHI decays are not intense and which do not cause major panel damage. Most simulations show that cumulative generations for these very frequent events (with return periods shorter than 3 years) are spread around the summer median (gray curves shown in Figure 4). Events with longer

return periods (above 3 years) are often driven by stronger storms. For example, reductions in generation with 10-year return periods are caused by hurricanes that reach a category of at least 3 in 14% of counties. Yet, reductions with 1000-year return periods are caused by at least category-3 hurricanes in 42% of counties. These less frequent events will significantly affect cities' abilities to harvest solar power through both strong GHI decays due to optically thick clouds absorbing and reflecting light and extreme winds leading to solar panel damage and failure. Note that cloud conditions of category-5 hurricanes drastically reduce the median GHI by 74%, i.e., $f_4 = -0.34$, even at distant sites 0.5ROCI away from the hurricane center (Figure 3). Few realizations with failed solar panels stand out as cumulative generation is flat after failure (Figure 4).

Figure 4 also demonstrates how different geographical locations have different risks of reduced solar generation. The results indicate that in New York City, NY, an event with a 1000-year return period will not lead to solar panel failure, but due to hurricane clouds, generation would be similar to the one during the winter. In contrast, in New Hanover, NC, an event with a 1000-year (or 333-year) return period will lead to complete loss of generation triggered by solar panel failure almost as soon as the hurricane makes landfall. Miami-Dade, FL, and Galveston, TX, face higher risk as even an event with a 100-year return period can reduce their solar generation capacity to negligible levels.

To comprehensively visualize the spatial distribution of risk of losing solar generation, Figure 5 shows cumulative solar generation at day 4 after landfall for multiple return periods as a percentage of the median generation during the summer. The plot shows that solar generation during an event with a 3-year return period will be reduced by around 25% on average for the counties in the analysis, with slightly higher reductions in Mid-Atlantic and the northern region of the South Atlantic. For example, the average reductions in New Jersey and South Carolina were 27% and 26%, respectively. Average reductions for events with 10-year and 33-year, 100-year, 333-year, and 1000-year return periods were 40%, 50%, 59%, 72%, and 82%, respectively. While events with return periods of 33 years and lower

are thoroughly controlled by GHI decay during cloud conditions, as noted earlier, events with 100-year return period can bring generation to 0 due to solar panel failure, especially in counties in the southern states, e.g., Texas, Louisiana, and Florida. Events with 333-year return periods lead to panel failures in counties that are even a hundred kilometers away from the coastline. Events with 1000-year return periods will expand the regions with panel failures triggering complete reduction of solar generation in almost entire states, e.g., 100% in Florida and 96% in Louisiana. These results show that northern and southern states undergo significant reductions in solar generation even for less frequent events (31% in Florida versus 40% in New Jersey for 10-year return period). However, rarer events will disproportionately exacerbate the generation reduction in the southern states as solar infrastructure fails at higher rates.

Discussion

This paper has proposed the first framework to evaluate solar generation during hurricanes at a regional scale. The framework integrates four key pieces: hurricane hazard analysis, solar irradiance modeling, solar panel vulnerability, and a newly presented model to assess irradiance decay as a result of hurricane cloud conditions. This framework aims to be the foundation for assessing the vulnerability of modern power systems with solar generation infrastructure to hurricanes and a tool to test strategies and policies to increase their resilience.

The integrative framework has been presented through a proposed algorithm to model the time-series of solar generation during hurricanes. While the algorithm is a key contribution from this article, our scope also includes the development of a model to capture irradiance decay during hurricanes, a crucial piece of the framework, which to the authors' knowledge, has not been developed before. The irradiance decay model is based on an extensive assessment of GHI under 22 landfalling storms in the North American basin, which reached a

category of at least 3 during their lifetime. The dataset conclusively shows that hurricanes reduce the GHI throughout their tracks. We confirmed that the distance from a site to the hurricane and its category are key predictors of the irradiance decay. We argue that the mechanism driving the decay is the formation of optically thick clouds in the eyewall, which often become thicker during hurricane intensification. These optically thick clouds, with high moisture density and vertical depth, reduce direct incident radiation by light absorption and reflection.

We fitted four functional forms that vary in complexity to represent irradiance decay using a mixed-effects regression. Multiple category-dependent features controlling the intensity and shape of decay were tested, and the best functional form was selected using AIC to demonstrate its suitable statistical performance. ROCI is shown to be an effective size metric for normalizing the distance in the functional forms of irradiance decay.

Finally, we described the algorithm to quantify solar generation during hurricanes. We apply the algorithm to 1217 counties belonging to 21 states in the Eastern region of the U.S.. We use cumulative generation at day four since landfall as a metric to measure resilience. Our results show that generation during most storms with return periods shorter than three years will be distributed as normal conditions during summer. In contrast, events with return period of 10 years and 33 years will reduce generation significantly, by 37% and 48%, on average, respectively. Optically thick clouds that reflect and absorb light are the drivers of such reductions. Rarer events (with return periods of 333 and 1000 years) will reduce generation to a higher degree. While in the northern states, these extreme events will reduce generation due to optically thick clouds, in the southern states, they will likely trigger solar panel structural failure due to strong winds. As a result, southern regions face a higher risk of losing power generation, as northern regions can still generate at a reduced level if the panel has not failed. Solar generation is expected to become a pillar for our future power systems. Thus, our results show that for communities to rely on this pillar to deliver critical power during extreme events, higher standards for solar panel structural design are required.

Acknowledgement

We acknowledge the financial support by the Andlinger Center for Energy and the Environment at Princeton University through the Distinguished Postdoctoral Fellowship. Additionally, this research was also supported by the NSF Grants 1520683 and 1652448. The authors are grateful for their generous support.

Supporting Information Available

The Supporting Information is available free of charge at the ACS website.

References

(1) Perea, A.; Smith, C.; Davis, M.; Mond, A.; Gallagher, B.; Rumery, S.; Holm, A.; Goldstein, R.; Baca, J. *U. S. Solar Market Insight Executive Summary*; 2019.

(2) Moriarty, P.; Honnery, D. Can renewable energy power the future? *Energy Policy* **2016**, *93*, 3–7.

(3) Solangi, K. H.; Islam, M. R.; Saidur, R.; Rahim, N. A.; Fayaz, H. A review on global solar energy policy. *Renewable and Sustainable Energy Reviews* **2011**, *15*, 2149–2163.

(4) Creutzig, F.; Agoston, P.; Goldschmidt, J. C.; Luderer, G.; Nemet, G.; Pietzcker, R. C. The underestimated potential of solar energy to mitigate climate change. *Nature Energy* **2017**, *2*.

(5) Devabhaktuni, V.; Alam, M.; Shekara Sreenadh Reddy Depuru, S.; Green, R. C.; Nims, D.; Near, C. Solar energy: Trends and enabling technologies. *Renewable and Sustainable Energy Reviews* **2013**, *19*, 555–564.

(6) Kannan, N.; Vakeesan, D. Solar energy for future world: - A review. *Renewable and Sustainable Energy Reviews* **2016**, *62*, 1092–1105.

(7) Campbell, R. J.; Clark, C. E.; Andrew Austin, D. *Repair or Rebuild: Options for electric power in Puerto Rico*; 2018; pp 45–102.

(8) Abatzoglou, J. T.; Smith, C. M.; Swain, D. L.; Ptak, T.; Kolden, C. A. Population exposure to pre-emptive de-energization aimed at averting wildfires in Northern California. *Environmental Research Letters* **2020**, *15*.

(9) Chediak, M.; Eckhouse, B.; Baker, D. R. California Braces for More Blackouts as Heat Wave Persists. 2020; `https://www.bloomberg.com/news/articles/2020-08-15/two-million-californians-go-dark-and-more-heat-is-coming`.

(10) Winkler, J.; Dueñas-Osorio, L.; Stein, R.; Subramanian, D. Performance assessment of topologically diverse power systems subjected to hurricane events. *Reliability Engineering and System Safety* **2010**, *95*, 323–336.

(11) Ouyang, M.; Dueñas-Osorio, L.; Min, X. A three-stage resilience analysis framework for urban infrastructure systems. *Structural Safety* **2012**, *36-37*, 23–31.

(12) Guikema, S. D.; Nateghi, R.; Quiring, S. M.; Staid, A.; Reilly, A. C.; Gao, M. Predicting Hurricane Power Outages to Support Storm Response Planning. *IEEE Access* **2014**, *2*, 1364–1373.

(13) González, A. D.; Dueñas-Osorio, L.; Sánchez-Silva, M.; Medaglia, A. L. The Interdependent Network Design Problem for Optimal Infrastructure System Restoration. *Computer-Aided Civil and Infrastructure Engineering* **2016**, *31*, 334–350.

(14) Feng, K.; Min, O.; Lin, N. The hurricane-blackout-heatwave compound hazard risk and resilience in a changing climate. *Nature Communications (In review)* **2020**,

(15) Patel, S.; Ceferino, L.; Liu, C.; Kiremidjian, A.; Rajagopal, R. The Disaster Resilience Value of Rooftop Solar in Residential Communities. *Earthquake Spectra* **2020**, *In Review*, 1–20.

(16) Ceferino, L.; Liu, C.; Alisjahbana, I.; Patel, S.; Sun, T.; Kiremidjian, A.; Rajagopal, R. Earthquake resilience of distributed energy resources. 17th World Conference on Earthquake Engineering. Tokyo, Japan, 2020.

(17) Sengupta, M.; Xie, Y.; Lopez, A.; Habte, A.; Maclaurin, G.; Shelby, J. The National Solar Radiation Data Base (NSRDB). *Renewable and Sustainable Energy Reviews* **2018**, *89*, 51–60.

(18) Landsea, C. W.; Franklin, J. L. Atlantic hurricane database uncertainty and presentation of a new database format. *Monthly Weather Review* **2013**, *141*, 3576–3592.

(19) Emanuel, K.; Sundararajan, R.; Williams, J. Hurricanes and global warming. *Bulletin of American Meteorological Society* **2008**, *89*, 347–368.

(20) Marsooli, R.; Lin, N.; Emanuel, K.; Feng, K. Climate change exacerbates hurricane flood hazards along US Atlantic and Gulf Coasts in spatially varying patterns. *Nature Communications* **2019**, *10*, 1–9.

(21) Chavas, D. R.; Lin, N.; Emanuel, K. A model for the complete radial structure of the tropical cyclone wind field. Part I: Comparison with observed structure. *Journal of the Atmospheric Sciences* **2015**, *72*, 3647–3662.

(22) Goodman, J. N. Performance Measures for Residential PV Structural Response to Wind Effects. Doctor of Philosophy, Georgia Institute of Technology, 2015.

(23) Watson, E. B. Modeling Electrical Grid Resilience under Hurricane Wind Conditions with Increased Solar Photovoltaic and Wind Turbine Power Generation. Doctor of Engineering, The George Washington University, 2018.

(24) Houze, R. A. Clouds in tropical cyclones. *Monthly Weather Review* **2010**, *138*, 293–344.

(25) Xie, Y.; Sengupta, M.; Dudhia, J. A Fast All-sky Radiation Model for Solar applications (FARMS): Algorithm and performance evaluation. *Solar Energy* **2016**, *135*, 435–445.

(26) Xie, Y.; Sengupta, M.; Wang, C. A Fast All-sky Radiation Model for Solar applications with Narrowband Irradiances on Tilted surfaces (FARMS-NIT): Part II. The cloudy-sky model. *Solar Energy* **2019**, *188*, 799–812.

(27) Nouri, B.; Wilbert, S.; Segura, L.; Kuhn, P.; Hanrieder, N.; Kazantzidis, A.; Schmidt, T.; Zarzalejo, L.; Blanc, P.; Pitz-paal, R. Determination of cloud transmittance for all sky imager based solar nowcasting Transmittance known Transmittance unknown. *Solar Energy* **2019**, *181*, 251–263.

(28) Lehr, J.; Vrettos, E.; Rajagopal, R.; Jain, R.; Everts, M. Financial Viability of Residential Photovoltaic and Battery Systems in Californias. *Journal of Management and Sustainability* **2017**, *7*, 16.

(29) Weatherford, C.; Gray, W. Typhoon Structure as Revealed by Aircraft Reconnaissance. Part II: Structural Variability. *Monthly Weather Review* **1988**, *116*, 1044–1056.

(30) Kokhanovsky, A. A.; von Hoyningen-Huene, W. Optical properties of a hurricane. *Atmospheric Research* **2004**, *69*, 165–183.

(31) John, J.; Shukla, B. P.; Gajjar, P. N.; Sathiyamoorthy, V. Study of satellite-derived cloud microphysical parameters for tropical cyclones over the North Indian Ocean (2010–2013). *Theoretical and Applied Climatology* **2020**, *139*, 1163–1173.

(32) Luo, Z.; Stephens, G. L.; Emanuel, K. A.; Vane, D. G.; Tourville, N. D.; Haynes, J. M. On the use of CloudSat and MODIS data for estimating hurricane intensity. *IEEE Geoscience and Remote Sensing Letters* **2008**, *5*, 13–16.

(33) Pinheiro, J.; Bates, D. *Mixed-Effect Models in S and S-PLUS*; Springer Science & Business Media, 2006.

(34) Campbell, K. W.; Bozorgnia, Y. NGA-West2 ground motion model for the average horizontal components of PGA, PGV, and 5% damped linear acceleration response spectra. *Earthquake Spectra* **2014**, *30*, 1087–1114.

(35) Abrahamson, N.; Gregor, N.; Addo, K. BC hydro ground motion prediction equations for subduction earthquakes. *Earthquake Spectra* **2016**, *32*, 23–44.

(36) Lindstrom, M. J.; Bates, D. M. Mixed Effects Models for Repeated Measures Data. *Biometrics* **1990**, *46*, 673–687.

(37) Lin, N.; Emanuel, K.; Oppenheimer, M.; Vanmarcke, E. Physically based assessment of hurricane surge threat under climate change. *Nature Climate Change* **2012**, *2*, 462–467.

(38) Emanuel, K. Assessing the present and future probability of Hurricane Harvey's rainfall. *Proceedings of the National Academy of Sciences of the United States of America* **2017**, *114*, 12681–12684.

(39) Vickery, P.; Skerlj, P. Hurricane Gust Factors Revisited. *Journal of Structural Engineering* **2005**, *131*, 825–832.

(40) Akaike, H. A new look at the statistical model identification. *IEEE Transactions on Automatic Control* **1974**, *19*, 716–723.

(41) Rouge, B.; Sciences, C.; Rouge, B. Spatiotemporal Patterns and Return Periods of Tropical Storm and Hurricane Strikes from Texas to Maine. **2006**, 3498–3509.

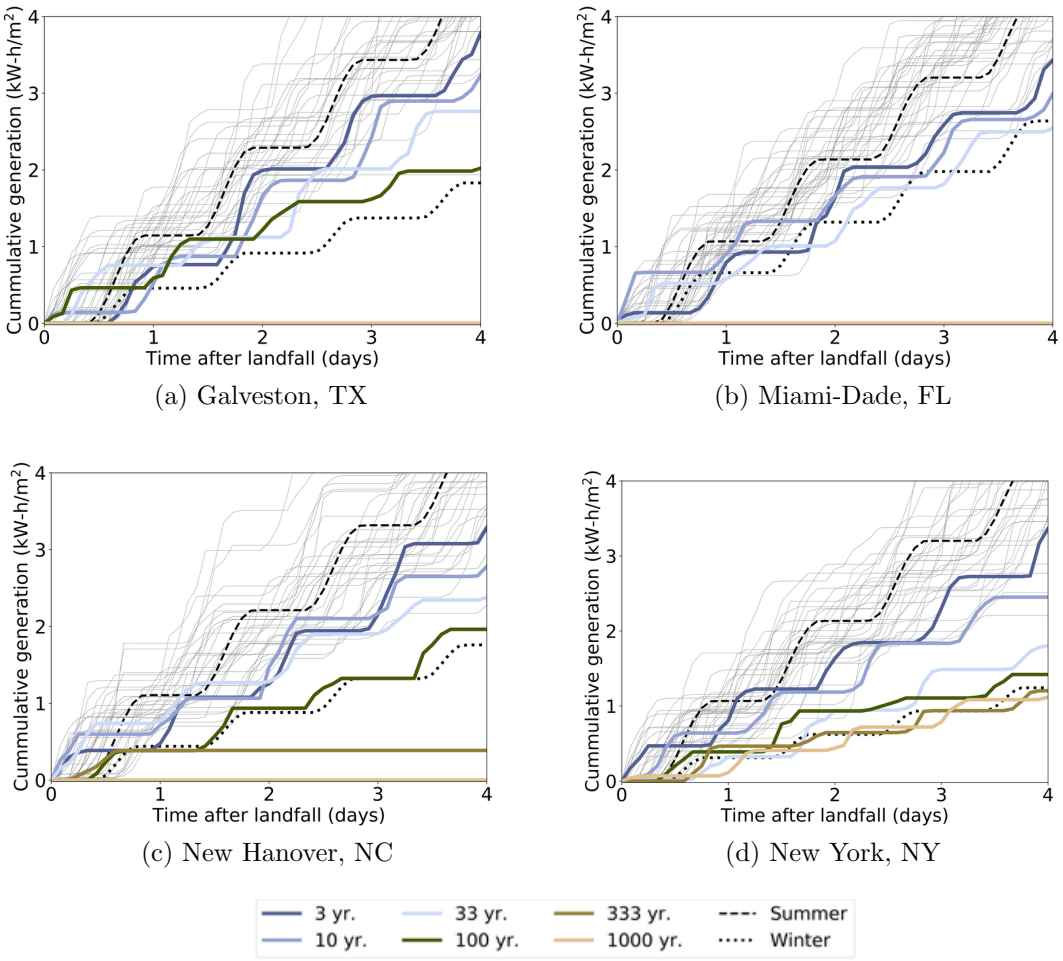

(a) Galveston, TX

(b) Miami-Dade, FL

(c) New Hanover, NC

(d) New York, NY

Figure 4: Simulations of cumulative generation from solar panels in four different counties through different hurricane conditions for four days. Only 50 out of the 5018 simulations are included in the plot for visual clarity. For reference, the cumulative of median solar generation during normal conditions (without hurricanes) in the months of January and July are shown.

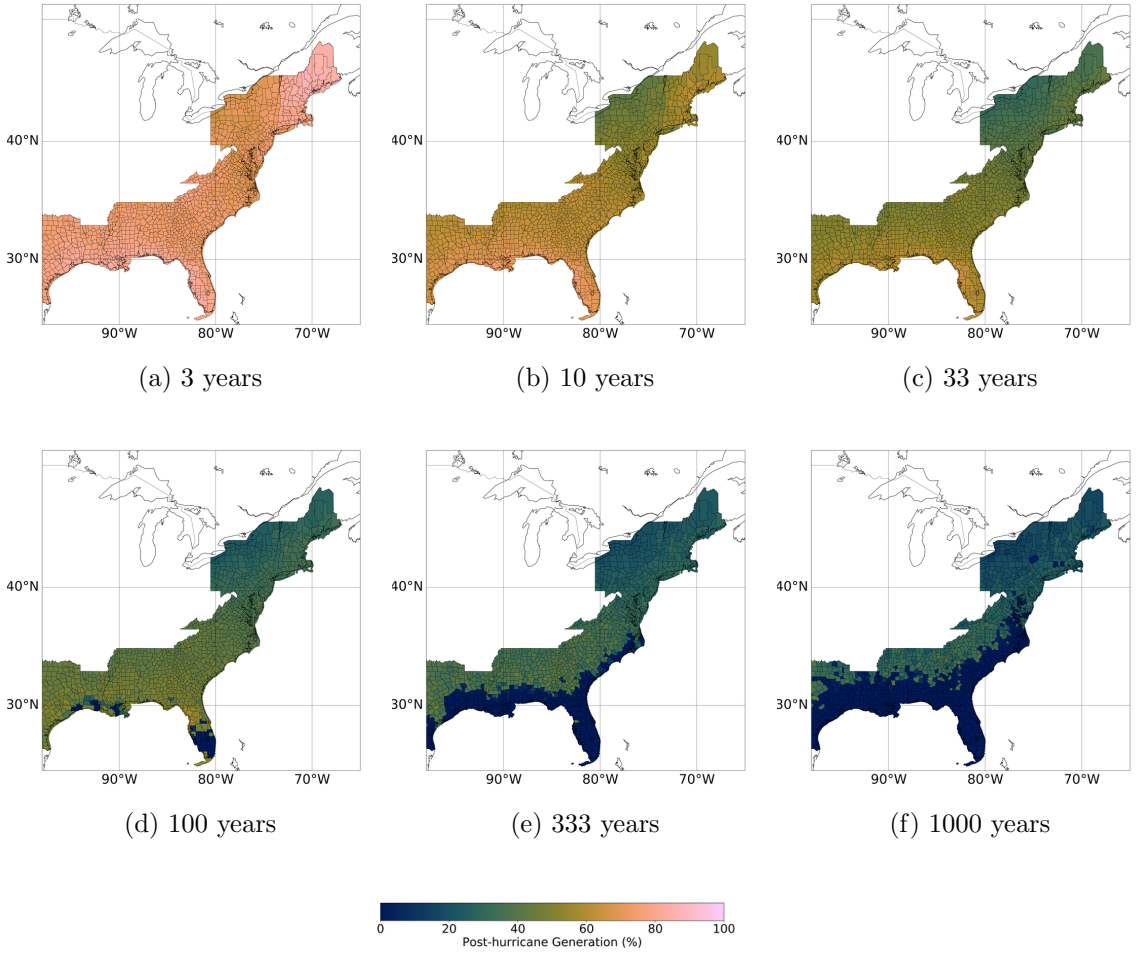

(a) 3 years (b) 10 years (c) 33 years

(d) 100 years (e) 333 years (f) 1000 years

Figure 5: Cumulative generation from solar panels for different levels of hurricane conditions at day four since landfall as a percentage of the median cumulative generation during the summer (July). Different levels of cumulative generations are characterized by different return periods, i.e., average time between storms that cause same or lower generation.